**Academic Journal of Science and Technology**
ISSN: 2771-3032 | Vol. 4, No. 1, 2022

# Fault Identification of Double-circuit Transmission Lines on The Same Tower Based on CEEMDAN-SSA-SVM

**Xi Zou[1, 2], Hong Song[3], Hao Wu[1, 2]**

[1]Automation and Information Engineering, Sichuan University of Science & Engineering, Zigong 643000, Sichuan, China
[2]Artificial Intelligence Key Laboratory of Sichuan Province, Sichuan 643000, Zigong, China
[3]ABA Teachers University, Sichuan,623002, Aba Prefecture, China

**Abstract:** In order to improve the reliability of double-circuit transmission lines on the same tower, by analyzing the variation law of inverse wave of fault voltage inside and outside the area, a support vector machine (SVM) method for internal and external fault identification of double-circuit transmission lines on the same tower based on adaptive noise complete ensemble empirical mode decomposition and sparrow search algorithm optimization is proposed. This method carries on the phase mode transformation of the current and voltage after the fault. The inverse wave current in the time window after the fault is adaptively decomposed by CEEMDAN, and the corresponding energy entropy is extracted to form the feature vector. The SMOTE algorithm is used to balance the fault samples outside the region. Finally, the feature vector set is input to the SSA-SVM classifier for training and testing. Through theoretical and simulation analysis, the following results are obtained: the algorithm in this paper is not affected by fault initial angle, transition resistance and fault distance.

**Keywords:** Double-circuit lines on the same pole, Reverse wave current, CEEMDAN, SMOTE algorithm, SSA-SVM, Fault identification.

## 1. Introduction

With the rapid growth of population in our country, the available land resources will be more and more scarce, and the double-circuit transmission lines on the same tower are widely used because of their small footprint, large transmission capacity and low erection cost[1]. Therefore, after the failure of the line, it is of great significance to find the fault point and clear it in time to reduce the property loss and restore the life quickly.

A large number of domestic and foreign scholars carry out research on double-circuit transmission lines on the same tower. According to the similarity relationship between forward wave current waveform on one side and reverse wave current waveform on the other side after the fault of double-circuit transmission lines on the same tower, a fault identification method for double-circuit transmission lines on the same tower based on waveform similarity is proposed in reference [2]. The transformation law of the initial traveling wave current at both ends of the line during internal and external faults is analyzed in reference [3]. The initial traveling wave current is decomposed into six layers by using the multi-resolution singular value algorithm, and the current integral of each layer is calculated as the eigenvector. The eigenvector is input to the random forest classifier to identify the faults inside and outside the area. The transverse differential protection of double-circuit lines on the same tower based on six-sequence fault components is proposed in reference [4]. The phase fault components are decomposed into six-sequence fault components, which eliminates the mutual inductance between phases and lines, and avoids the defects of traditional line selection components of transverse differential protection. The S transformation of bus voltage and line current is carried out in reference [5], the measured wave impedance of the line is calculated, the concepts of sum wave impedance and differential wave impedance are given, and the faults inside and outside the area are identified by comparing the comprehensive sum wave impedance and the comprehensive differential wave impedance. A fault identification of double-circuit transmission lines on the same tower based on the phase difference of initial traveling wave is proposed in reference [6]. The initial traveling wave phase is calculated by using S-transform. The protection criterion is constructed by analyzing the phase relationship of the initial current traveling wave on the same end and opposite end of the double-circuit line. In reference [7], a fault property criterion and comprehensive reclosing strategy based on out-of-phase coupling voltage characteristics are proposed for grounding fault, which can deal with the out-of-phase of healthy line, increase the amplitude of fault line coupling electrical quantity, and increase the accuracy of identifying the nature of non-cross-line grounding fault. Reference [8] aims at the problem that the traditional reclosing strategy does not determine the fault nature and causes the secondary impact on the system due to the blind reclosing and the failure of reclosing. Based on the reactive power of fault phase, an adaptive reclosing strategy for cross-line grounding fault of double-circuit transmission lines with parallel reactors is proposed. According to the reference [9], due to the influence of mutual inductance between double-circuit lines on the same pole, the grounding distance protection of single-interval electrical quantity has some problems, such as inaccurate measurement of fault line distance, reverse direction mis operation of non-fault lines and terminal fault overstep. The zero-sequence compensation coefficient is adaptively selected by using the circuit breaker position and grounding switch position information of double-circuit lines, and the fault line and phase selection are realized by using six-phase current information and six-sequence component method of double-circuit lines. according to the line selection results, the adaptive compensation of the adjacent line zero sequence current of the grounding distance protection of the fault line is realized, but the adjacent line zero sequence current compensation is no longer used for the non-fault line.

In reference [10], when a fault occurs, the branch is identified by comparing the voltage amplitude of the connection point. Then, according to the identification results, the two-terminal method is used to calculate the fault location, and finally the fault distance of the fault branch is obtained.

# 2. Analysis of Traveling Wave Transmission Characteristics

The model of double-circuit transmission line on the same pole is shown in figure 1, and M and N are the buses at both ends of the line. $L_1$ And $L_2$ for the protection line within the area; $L_3$ and $L_4$ for the protection line outside the area; $R_1$ - $R_6$ for the protection detection unit inside and outside the area.

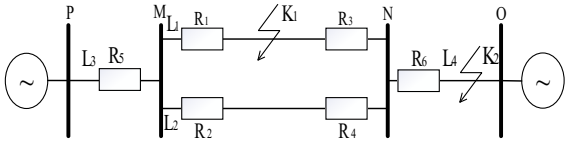


**Figure 1.** Model of double-circuit transmission line on the same tower

## 2.1. Fault analysis of single circuit in the area

Taking a single-circuit fault line as an example, the transient traveling wave transmission process occurs when a fault occurs at $K_1$ as shown in figure 2.

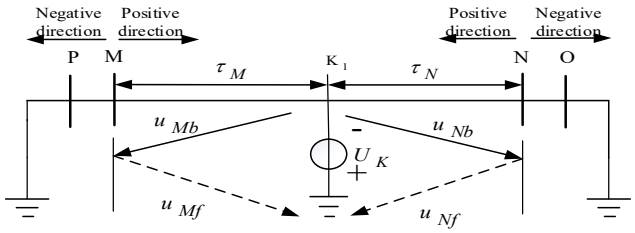


**Figure 2.** Traveling wave transmission process of single-loop fault in the area

$\tau_M$ and $\tau_N$ are the time for the transient traveling wave to be transmitted to both ends at the point of failure, and the total transmission time at both ends is $\tau$ . $u_{Mf}$ and $u_{Nf}$ are forward wave signals, $u_{Mb}$ and $u_{Nb}$ are inverse wave signals. As can be seen from the analysis of figure 2, when a fault occurs, the inverse wave signals $u_{Mb}$ and $u_{Nb}$ are first detected in the M and N protection units. If the inverse wave time detected at one end of the line is t, the other end can detect the inverse wave within $[t, t+\tau]$ time.

## 2.2. Out-of-zone fault analysis

When a fault occurs in $K_2$ , the transient traveling wave transmission process is generated by the fault outside the area as shown in figure 3. When a fault occurs, the $u_{Nf}$ forward traveling wave is detected in the N terminal traveling wave unit, the traveling wave transmission process will not be interrupted, $u_{Nf}$ can be transmitted all the way to M terminal, $u_{Nf}$ becomes $u_{Mb}$ inverse wave at M terminal, $u_{Mb}$ will be reflected and transmitted at the physical boundary of M terminal, $u_{Mb}$ becomes $u_{Mf}$ forward wave after reflection, $u_{Mf}$ forward wave will be transmitted to N terminal without interruption on the line, and finally $u_{Mf}$ forward wave will become N terminal $u_{Nb}$ retrograde wave.

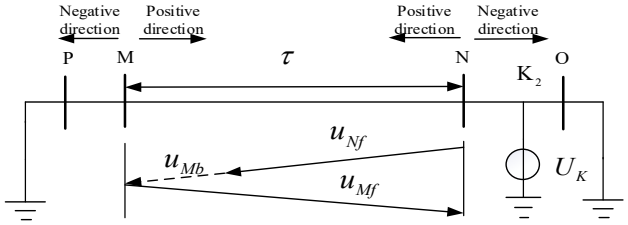


**Figure 3.** Transient traveling wave transmission process of fault outside the zone

According to the analysis of figure 3, when a fault occurs outside the area, if the detection time of forward traveling wave $u_{Nf}$ at N terminal is t, then within $[t, t+2\tau)$ , inverse wave $u_{Nb}$ can not be detected at N terminal theoretically, while inverse wave $u_{Nb}$ can be detected at M terminal.

## 2.3. Calculation formula of inverse traveling wave

Formula (1) is the calculation formula of voltage inverse wave at both ends:

$$\begin{cases} u_{Mb} = \frac{1}{2}(u_M - Z_c i_M) \\ u_{Nb} = \frac{1}{2}(u_N - Z_c i_N) \end{cases} \tag{1}$$

In the above formula: $Z_c$ is the uplink wave impedance of the line, $u_M$ , $u_N$ , $i_M$ , $i_N$ is the voltage and current at both ends.

# 3. Algorithm Realization

## 3.1. Phase mode transformation

There are a large number of coupling phenomena in the double-circuit transmission line on the same tower. in order to reduce its influence on the transmission line, the decoupling matrix is used to decompose the line into an independent single-phase system. Formula (2) shows the phase mode transformation matrix [11].

$$M = \frac{1}{15}\begin{bmatrix} 5 & 5 & 5 & 5 & 5 & 5 \\ 5 & -1 & -4 & 5 & -1 & -4 \\ 5 & -4 & -1 & 5 & -4 & -1 \\ 5 & 5 & 5 & -5 & -5 & -5 \\ 5 & -1 & -4 & -5 & 1 & 4 \\ 5 & -4 & -1 & -5 & 4 & 1 \end{bmatrix} \tag{2}$$

Formula (3) is its phase mode transformation relation:

$$\begin{aligned} &[u_{1A} \quad u_{1B} \quad u_{1C} \quad u_{2A} \quad u_{2B} \quad u_{2C}] \\ &= M\,[u_{T0} \quad u_{T1} \quad u_{T2} \quad u_{F0} \quad u_{F1} \quad u_{F2}] \end{aligned} \tag{3}$$

In the above formula: $u_{T0}, u_{T1}, u_{T2}, u_{F0}, u_{F1}, u_{F2}$ is 0 mode, 1 mode and 2 modulus voltage in the same direction

and in the opposite direction, respectively.

## 3.2. CEEMDAN algorithm

The implementation process of CEEMDAN algorithm is as follows:

(1) consistent with EEMD, the signal $X(t)+\varepsilon_0 n^i(t)$ is decomposed N times by EMD in CEEMDAN algorithm, and the first modal component is obtained by mean calculation.

$$\overline{IMF_1(t)}=\frac{1}{N}\sum_{i=1}^{N}IMF_1^i(t) \tag{4}$$

(2) calculate the first margin signal $r_1(t)$ :

$$r_1(t)=X(t)-\overline{IMF_1(t)} \tag{5}$$

(3) the signal $r_1(t)+\varepsilon_1 E_1(n^i(t))$ is decomposed repeatedly for N times by EMD algorithm, and the second modal component is obtained.

$$\overline{IMF_2(t)}=\frac{1}{N}\sum_{i=1}^{N}E_1(r_1(t)+\varepsilon_1 E_1(n^i(t))) \tag{6}$$

(4) for $k=2,\mathrm{B}\ ,K$ , calculate the first residual signal:

$$r_k(t)=r_{k-1}(t)-\overline{IMF_k(t)} \tag{7}$$

(5) repeat the calculation process of step (3), and get that the k + 1 modal function is:

$$\overline{IMF_{(k+1)}(t)}=\frac{1}{N}\sum_{i=1}^{N}E_1(r_k(t)+\varepsilon_k E_k(n^i(t))) \tag{8}$$

(6) repeat steps (4) and (5) until the residual signal satisfies the termination condition of decomposition, and finally K modal components are obtained. The final residual signal of decomposition is:

$$R(t)=X(t)-\sum_{k=1}^{K}\overline{IMF_k(t)} \tag{9}$$

Eventually, the original signal can be decomposed into:

$$X(t)=R(t)+\sum_{i=1}^{K}\overline{IMF_k(t)} \tag{10}$$

## 3.3. Fault simulation analysis

### 3.3.1. Simulation and analysis of faults in the area

The waveforms within $[\tau,2\tau)$ time after the occurrence of short-circuit grounding fault in phase B and C of line $L_2$ in the area are shown in figure 4, and figures 5 and 6 are CEEMDAN decomposition waveforms. As can be seen in figure 4, signals can be detected at both ends within $[\tau,2\tau)$ times.

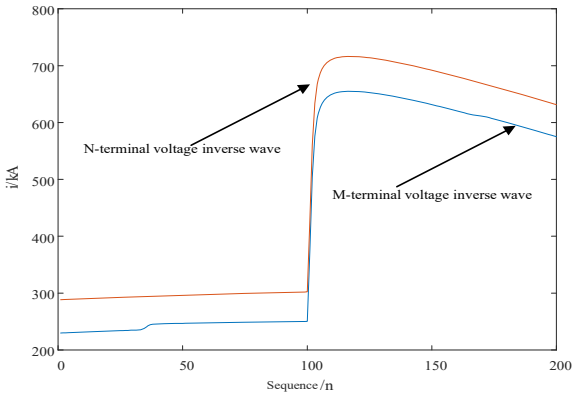


**Figure 4.** Reverse voltage waveform at both ends of the fault in the area

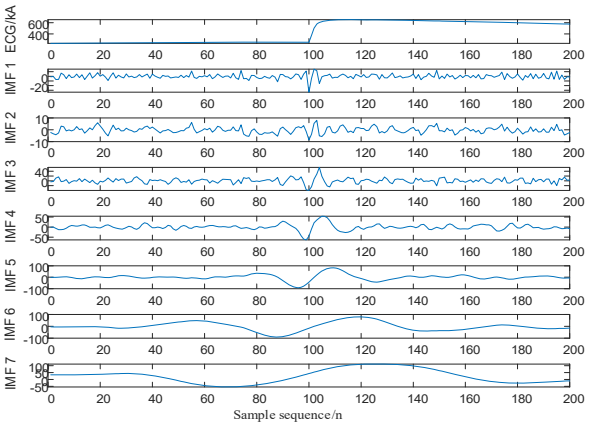


**Figure 5.** Decomposition waveform of fault M-terminal CEEMDAN in area

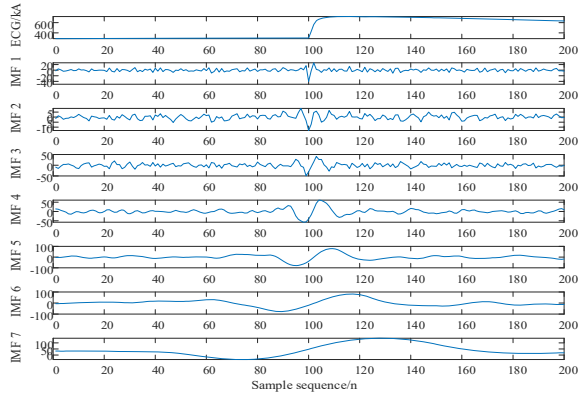


**Figure 6.** Decomposition waveform of fault N-terminal CEEMDAN in the area

### 3.3.2. Simulation analysis of out-of-zone fault

The waveform in $[\tau,2\tau)$ time after the occurrence of phase B and C short-circuit grounding fault outside the zone is shown in figure 7, and figures 8 and 9 are CEEMDAN decomposition waveforms. As can be seen in figure 7, there is one end that cannot detect the signal in $[\tau,2\tau)$ time.

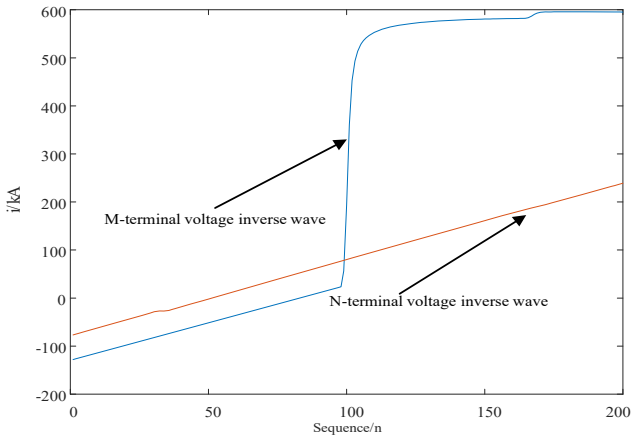


**Figure 7**. Reverse voltage waveforms at both ends of the fault outside the zone

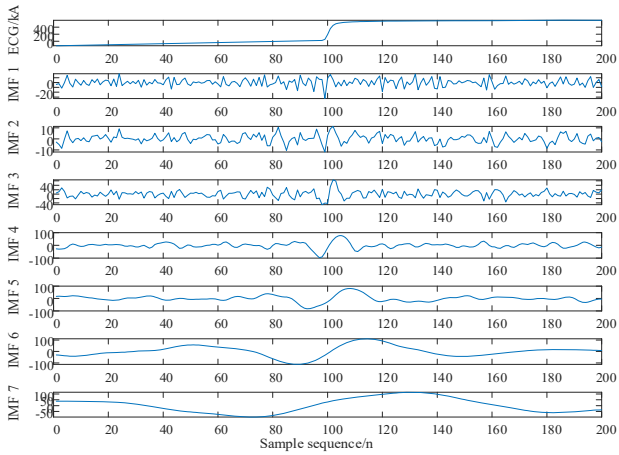


**Figure 8.** Decomposition waveform of M-terminal CEEMDAN of external fault

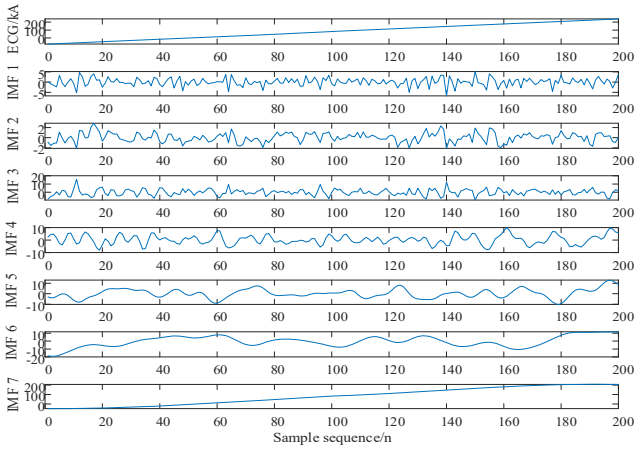


**Figure 9**. N-terminal CEEMDAN decomposition waveform of external fault

## 3.4. Energy entropy

The formula for calculating energy entropy is as follows:

$$\begin{cases} E_{Mn} = \int_{t=t_0+\tau}^{t_0+2\tau} \left| W_{Mn}(t) \right|^2 \\ E_{Nn} = \int_{t=t_0+\tau}^{t_0+2\tau} \left| W_{Nn}(t) \right|^2 \end{cases} \tag{11}$$

In formula (11), the nth IMF energy values of both ends are $E_{Mn}$ and $E_{Nn}$, and the nth signal transformation coefficients of both ends are $W_{Mn}(t)$ and $W_{Nn}(t)$ . The transmission time between the two ends is $\tau$ ; $\tau$ is 1ms.

$$\begin{cases} H_{Mi} = -\sum_{i=1}^{n} p_i \lg p_i \\ H_{Ni} = -\sum_{i=1}^{n} q_i \lg q_i \end{cases} \tag{12}$$

In formula (12): $p_i = E_i / E$ and $q_i = E_i / E$ are the percentage of the energy of the 1th $IMF_i$ to the total energy E after decomposition at both ends, respectively. $i = 1,2,\mathrm{B},5$, $H_{Mi}$ and $H_{Ni}$ denote the energy entropy of the $IMF$ after the decomposition of M and N, respectively.

# 4. Fault Recognition of Support Vector Machine Based on Sparrow Search Algorithm Optimization

## 4.1. SMOTE algorithm

SMOTE algorithm is usually used to deal with sample unbalanced data, and its idea is to use random linear interpolation in a small number of adjacent samples to increase the number of samples. The calculation formula is as shown in formula (13):

$$p_j = p_i + rand(0,1) \times (p_j - p_i) \tag{13}$$

In the formula: $rand(0,1)$ represents a random number between $(0\ 0\ 1)$ ; $p_j$ is an extended sample after SMOTE algorithm, $j = 1,2,\ldots,l$ .

## 4.2. Sparrow search algorithm optimizes support vector machine

### 4.2.1. Sparrow search algorithm

Sparrow search algorithm [12] the optimization steps are as follows:

The maximum fitness value of the sparrow is selected as the discoverer, and the formula (14) is used to update its position.

$$X_{i,j}^{t+1} = \begin{cases} X_{i,j}.\exp(-\dfrac{i}{\alpha.D}), if\ R_2 < ST \\ X_{i,j} + Q \times L, if\ R_2 \geq ST \end{cases} \tag{14}$$

In the formula: $j = 1,2,3,\mathrm{B}\ ,d$ ; D is the maximum number of iterations of the algorithm; $X_{i,j}$ is the position of the dimension j corresponding to Sparrow i; $R_2$ and $T$ represent the warning value and safety threshold, respectively.

Select the rest of the sparrows as participants, and use the formula (15) to update their positions.

$$X_{i,j}^{t+1}=\begin{cases} Q.\exp(\dfrac{X_w-X_{i,j}^t}{\alpha D}), if\ i>n/2 \\ X_P^{t+1}+\left|X_{i,j}-X_P^{t+1}\right|A^{+}L, otherwise \end{cases} \quad (15)$$

In the formula: $X_p$ is the best position corresponding to the discoverer sparrow type, and $X_{worst}$ is the worst position corresponding to the discoverer sparrow type.

The scout in the sparrow is randomly selected and updates its position using formula (16).

$$X_{i,j}^{t+1}=\begin{cases} X_{best}^t+\beta.\left|X_{i,j}^t-X_{best}^t\right|, if\ \ f_i>f_b \\ X_{i,j}^t+K.(\dfrac{\left|X_{i,j}^t-X_{worst}^t\right|}{(f_i-f_w)+\varepsilon}), if\ \ f_i=f_b \end{cases} \quad (16)$$

In the formula: $X_{best}$ represents the best X position corresponding to the Sparrow type of the scout, and β represents the improved control parameters before the algorithm.

#### 4.2.2. Support vector machine

The steps of the support vector machine algorithm are as follows:

Set up a sample $(x^i, y^i)$, $i=1,2,\mathtt{B}\ ,m,\ y^i\in\{-1,+1\}$, $x^i$ is the eigenvector, $y^i$ is the category label, The decision equation of classification plane can be expressed as follows:

$$f(x)=\omega^T x+b \quad (17)$$

Use the hyperplane to distinguish different types of samples: When $\omega^T x+b<0$ ,Classify the samples into category-1; When $\omega^T x+b>0$ ,Classify the samples into category-1.

For a given training set, the goal is to find the corresponding ω and b, so that the distance between the support vector and the classification plane can be furthest. The convex optimization of the objective function is carried out, and combined with the constraints, the problem can be transformed into the following optimization problems with constraints.

$$\begin{aligned} &\min_{\omega,b}\frac{1}{2}\|\omega\|^2+C\sum_{i=1}^{m}\xi_i; \\ &s.t.y^i.(\omega^T x+b)\geq 1, \end{aligned} \quad (18)$$

In the formula, C is the penalty coefficient and ξ is the relaxation factor, which is used to reduce the influence of samples which are difficult to classify and prevent overfitting.

Construction of Lagrange function based on the constrained Model of pair (18) The introduction of Lagrange multiplier $a_i(i=1,2,\mathtt{B}\ ,m)$ is as follows:

$$L(\omega,b,a)=\frac{1}{2}\|\omega\|^2-\sum_{i=1}^{m}a_1[y^i.(\omega^T x^i+b)-1] \quad (19)$$

By solving the dual problem, the optimal Lagrange multiplier $a^*$ and parameter $b^*$ are obtained, and the kernel function is introduced to obtain the final decision equation of the classifier as follows:

$$f(x)=\omega^T x+b=\sum_{i=1}^{m}a_i^* y^i K(x^i,x)+b^* \quad (20)$$

The common kernel functions are Gaussian kernel function and linear kernel function.

### 4.3. Fault identification process

Figure 10 shows the flow chart of the fault identification algorithm:

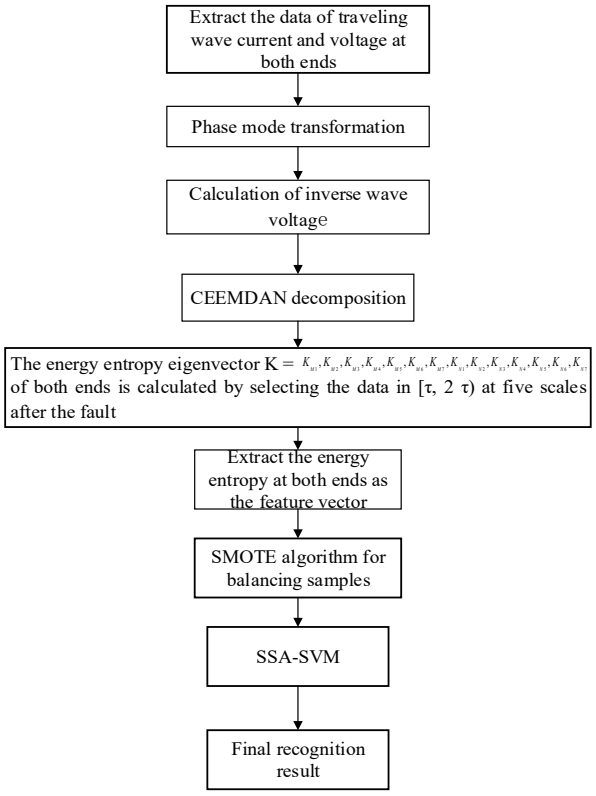


**Figure 10.** Flow chart of fault identification algorithm

## 5. Simulation verification

The simulation model is built on PSCAD, and the model of double-circuit transmission line on the same tower is shown in figure 1. The length of MN line is 300km and the length of PN line is 150km.

The sampling frequency of the system is 200kHz, the voltage level is 500kV and the frequency is 50Hz.

### 5.1. Training sample composition

For example, Table 1 sets the parameters for the training sample.

**Table 1.** Fault setting of training samples

| Fault situation | Local fault | Out-of-zone fault |
|---|---|---|
| Fault initial angle | 10 species | 110 species |
| Transition resistance | 150Ω | 300Ω |
| Fault type | 117 species | 11 species |
| Fault distance | Distance from N-terminal 150km | Distance from N-terminal 100km |
| Fault sample | $117\times10=1170$ groups | $11\times10=110$ groups |

After balancing the out-of-zone samples, 1100 groups of out-of-zone fault samples are obtained, and 2270 groups of eigenvectors are input to the SSA-SVM network for training.

## 5.2. Recognition result of training set

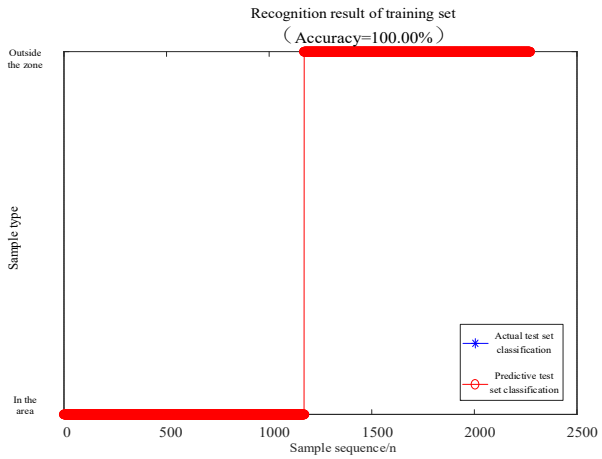


**Figure 11.** Recognition result of training set

The recognition effect of the training set is shown in figure 11, and it can be seen from the figure that the recognition result of the training set is better.

## 5.3. \ Algorithm testing

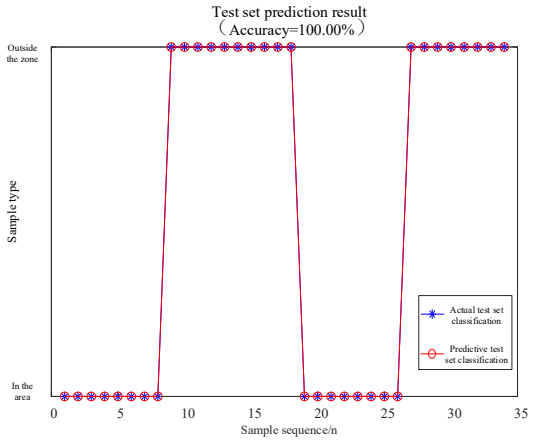


**Figure 12.** Test prediction results

As shown in figure 12, the test prediction results show that the algorithm is not affected by fault initial angle, transition resistance and fault distance.

# 6. Concluding Remarks

In this paper, by analyzing the voltage retrograde waveform in the time window after the fault inside and outside the area, a fault identification method of copper drum double-circuit transmission line based on CEEMDAN+SSA-SVM is proposed. Through theoretical and simulation analysis, it is concluded that the algorithm in this paper is not affected by fault initial angle, transition resistance and fault distance.

# References


[1] Zhu Yiyuang ,Du Hongji, Zhao Qingchun. Research on phase selection for double circuit lines on the same tower with asymmetrical parameters [J]. Power System Protection and Control,2017,45(15):133-139.

[2] Yang Liang, Wu Hao, Li Dong, et al. Fault identification of double-circuit lines on the same pole based on waveform similarity [J]. Journal of Sichuan University of Light and Chemical Engineering (Natural Science Edition), 2021, 34 (06): 71-78.

[3] Yang Liang, Wu Hao, Hu Xiaotao, et al. Fault identification of double-circuit lines on the same tower based on MRSVD-RF [J]. Journal of Electric Power Systems and Automation, 2022 Journal 34 (01): 65-75.

[4] Wang Zeyang. Transverse differential directional protection for double-circuit lines on the same tower based on six-sequence fault components [J]. Communication Power supply Technology, 2019-36 (12): 12-14.

[5] Ye Ruikai, Wu Hao, Dong Xing. Fault identification of double-circuit transmission lines on the same tower based on measuring wave impedance [J]. Journal of Zhejiang University (Engineering Science), 2019,53(12):2412-2422

[6] Ye Ruikai, Wu Hao, Dong Xing. Fault identification of double lines on the same tower based on phase difference of initial traveling wave [J]. Protection and Control of Power system, 2019,47(03):118-128.

[7] Liang Luming, Li Fengting, Jie Chao, et al. Open-phase Coupling voltage feature based comprehensive reclosure for double-circuit lines non-line-to-line fault [J]. Power system Protection and Control, 2019,47(13):62-69.

[8] Zhou Weiji, Li Fengting, Jie Chao. Adaptive autoreclosing scheme for line-to-line grounded faults on double-circuit transmission lines with shunt reactors [J]. Power System Protection and Control,2022,50(01):33-41.

[9] Gao Houlei, Liu Yiqing, Wang Xingguo, et al. Optimization scheme of grounding distance protection based on station domain information for double-circuit lines on the same tower [J]. Electric Power Automation Equipment, 2021,41(03):49-56.

[10] Shoupeng Wang, Dongmei Zhao, Liqun Shang. Fault Location for Incomplete-Journey Double-Circuit Transmission Lines on Same Tower Based on Identification of Fault Branch[J]. Journal of Electrical Engineering & Technology, 2017, 12(5).

[11] Wang Yongjin, Fan Yanfang. Longitudinal protection method based on reverse wave and signal processing for UHVDC transmission line [J]. Electric Power Automation Equipment, 2020,40(03):114-121.

[12] Zhao Haiyang, Huang Jun, Wang Jindong, et al. Improved SSA-VMD algorithm and its application in fault diagnosis of reciprocating compressor [J]. Lubrication Engineering, 2022,47(7):147-152.